

Physics potential of timing layers for future detectors

S.V. Chekanov^a, A.V. Kotwal^c, C.-H. Yeh^b, S.-S. Yu^b

^a *HEP Division, Argonne National Laboratory, 9700 S. Cass Avenue, Argonne, IL 60439, USA.*

^b *Department of Physics and Center for High Energy and High Field Physics, National Central University, Chung-Li, Taoyuan City 32001, Taiwan*

^c *Department of Physics, Duke University, USA*

Abstract

The physics potential of timing layers with a few tens of pico-second resolution for calorimeters of future detectors in collider experiments is explored. The presented studies show how such layers can be used for identification of separate particles, as well as illustrate the benefit of detecting new event signatures beyond the Standard Model.

Keywords:

1. Introduction

Future experiments, such as CLIC [1], International Linear Collider (ILC) [2], high-energy LHC (HE-LHC), future circular pp colliders of the European initiative, FCC-hh [3] and the Chinese initiative, SppC [4] will require high precision measurements of particles and jets at large transverse momenta. The usage of timing information for such experiments can provide additional information that can be used to improve particle and jet reconstruction, as well as to reduce background events. For example, high-precision timing will be beneficial for b-tagging for all post-LHC experiments. For CLIC and FCC, high-precision time stamping of calorimeter energy deposits will be essential for background rejection (i.e. fake energy deposits) and pile-up mitigation. Precise timing information is important for improving reconstruction of particle flow objects by reducing overlap of energy showers in highly-granular calorimeters.

From the physics point of view, timing layers can be used for detection of long-lived particles and identification of standard model (SM) particles. At this moment, conceptional design reports for future experiments have not yet fully explored the benefits of the time of flight (TOF) measurements with tens-of-picosecond resolutions for calorimeters.

In this paper we will investigate the benefits of the timing layers with the resolution in the range 10 ps – 1 ns for identification of SM particles. The resolution of 1 ns is standard for the existing and planned calorimeters [1, 2, 3, 4], and is only used as a benchmark for comparisons with more challenging 10 – 20 ps resolution devices. In addition, we investigate the capabilities of timing layers for identification of heavy stable

Email addresses: chekanov@anl.gov (S.V. Chekanov), ashutosh.kotwal@duke.edu (A.V. Kotwal), a9510130375@gmail.com (C.-H. Yeh), syu@cern.ch (S.-S. Yu)

Preprints: Elsevier

March 23, 2020

particles which may be produced beyond the standard model (BSM). We hope such studies can help shape the requirements for future calorimeters, which were already outlined in the CPAD report [5] that emphasized the need to develop fast timing readout for calorimeter measurements.

2. Proposal

A generic design of hadronic (electromagnetic) calorimeters for future particle collision experiments (HE-LHC, FCC, CLIC, ILC etc.) is based on two main characteristics: (1) high-granularity electromagnetic (ECAL) and hadronic (HCAL) calorimeters with cells ranged from $3 \times 3 \text{ mm}^2$ to $5 \times 5 \text{ cm}^2$. (2) timing with a nanosecond precision that improves background rejection, vertex association, and detection of new particles. According to the CPAD report [5], a development of “picosecond time resolution” for future calorimeters is one of the critical needs. Presently, high-granularity calorimeters with > 1 millions channels and with tens of pico-second resolution represent a significant challenge due to the large cost.

As a part of the HL-LHC upgrade program, CMS and ATLAS experiments are designing high-precision timing detectors with the time resolution of about 30 ps [6, 7]. They are based on silicon sensors that add an extra “dimension to event reconstruction.

As discussed above, such timing capabilities have not been fully explored for future detectors beyond the HL-LHC upgrade. In particular, the baseline designs of the ECAL and HCAL of the CLIC/FCC detectors have not been optimized for precision timing in the range of a few tens of picoseconds. The latter is considered as an expensive option for many millions of the channels of these highly granular detectors. This opens an opportunity to investigate a cost-effective “timing layer” (with the time resolution of smaller than 30 ps) for the post-LHC detectors. This layer will be installed in front of high-granularity calorimeters, covering both the forward and barrel regions.

In this paper we will investigate the physics advantages of installing timing layers in the front of calorimeters of the post-LHC experiments. Typically, thin detectors in front of calorimeters are called “preshower”, and they have been previously installed for the ZEUS, CDF, ATLAS and CMS experiments. The design goal of such detectors is to count the number of charged particles in order to correct for energy losses. The timing information of “MIP” (minimum ionizing particles) is not used for particle identifications, nor precise timing. Unlike the standard preshower detectors, we propose to not only count MIP signals, but also reconstruct high-precision timing and the position of the MIPs. This timing detector will have a similar granularity as the proposed high-granularity electromagnetic calorimeters, but will have the sensor technology and the readout that are best suited for time stamping of MIP signals. Our proposal is to enclose the EM detectors with two timing layers, one - before the first EM layer, and the other is after the last ECAL layer (but before the HCAL). The two layers of the timing detector allow a robust identification of time stamps by correlating the position and time of the particles passing through the ECAL.

In this paper we will explore this idea using a semi-analytical approach and Monte Carlo simulations. A schematic representation of the positions of the timing layers for a generic detector geometry is shown in Fig. 1. In the following, the first timing layer

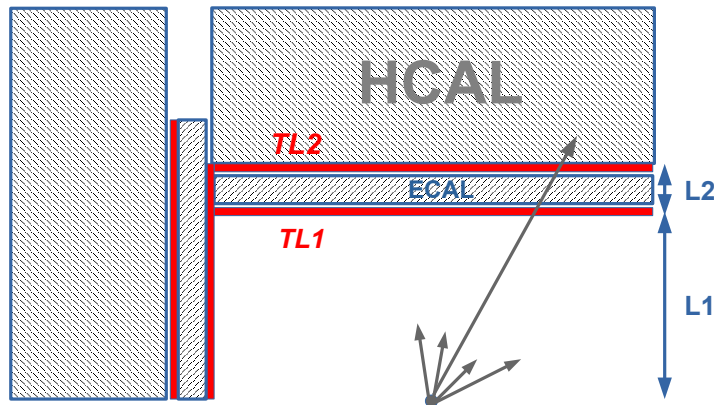


Figure 1: An example of positions of the thin timing layers for a generic detector. The thin timing layers will enclose the electromagnetic calorimeter, allowing a reliable reconstruction of the MIP signals with a timing resolution of the order of 10 ps.

74 (closest to the interaction point) will be called TL1, while the second timing layer after
 75 the electromagnetic calorimeter will be called TL2.

76 There are several reasons why the second timing layer (TL2) can be useful:

- 77 • It can be used to measure the TOF between TL2 and TL1 for identification
 78 of stable massive particles without known production vertex. This is especially
 79 important for the BSM models predicting stable heavy particles decaying close
 80 to the surface of the electromagnetic calorimeter.

81 For a typical ECAL based on the silicon technology, the distance between TL2 and
 82 TL1 is 0.2 – 0.4 m (depending on the calorimeter design). It is not immediately
 83 obvious that such a small distance can be used for physics measurements. A
 84 particle traveling with the speed of light can cross the distance between TL1 and
 85 TL1 within ~ 1 ns. As we will discuss later, this distance is sufficient to provide a
 86 large acceptance for heavy particle identification assuming a 10 – 20 ps detectors.

- 87 • The second layer is useful in the cases when a long-lived particle (neutral or
 88 charged) is produced without precise knowledge of the primary vertex (0,0,0) due
 89 to the beam (or pileup) smearing.

- 90 • It allows to correlate the hits with the first layer, and thus provides directionality
 91 of the hits. This feature can be useful to match the hits with the calorimeter cells
 92 and to deal with back-scatter hits which are typically arriving from the hadronic
 93 calorimeter at later time.

- It provides the redundancy for the calculation of TOF using the distance from the interaction point which can be determined using tracks.

The second layer of the timing detector can be justified if the recorded time difference between the first and the last ECAL layers of the electromagnetic showers is not significantly different from that expected from a particle traveling with the speed of light. If the travel time is significantly affected by large fluctuations caused by electromagnetic showers, second timing layer cannot effectively be used.

In order to verify this point, we used a full Geant4 (version 10.3) [8] simulation of the SiFCC detector [9] that allows to use the information of the ECAL hits. This detector design has an ECAL built from a highly segmented silicon-tungsten cells with the transverse size of 2×2 cm. The ECAL has 30 layers of tungsten pads with silicon readout, corresponding to $35 X_0$. The first 20 layers use tungsten of 3 mm thickness. The last ten layers use tungsten layers of twice the thickness, and thus have half the sampling fraction. The distance between the centers of the last and first ECAL layer is about 240 mm.

To verify that the time differences between the last and the first ECAL layer is close to the time required for a particle that travels with the speed of light, and can be neglected for the timing layers that have a timing resolution of the order of 1 ns, a sample of single pions (π^\pm) was created with 1 and 10 GeV momentum, respectively. The pseudorapidity for all pions was $\eta = 0$ (central region). The particles were reconstructed in the ECAL calorimeter, and the time difference $\Delta T = T_{\text{last}} - T_{\text{first}}$ of the hits between the last and first ECAL layers was calculated. Only the hits arriving first in time were considered since the electronics typically register¹ the fastest hits (while slower hits can be saved in pipeline buffers).

Figure 2 shows the time distribution of first arriving hits for 1 and 10 GeV pions. It can be seen that the peak positions of the distributions are smaller than 1 ns, as expected for the distance of about 20 cm between the centers of the last and first ECAL layers. Therefore, the hits registered by TL1 and TL2 will be simultaneous for the standard 1 ns resolution readout. They will be fully correlated in time, and are identified as a single crossing particle.

If a resolution of the timing layer is of the order of 10 – 20 ps, a physics measurement of TOF would be possible. To check this, Figure 2 shows the hit distribution for (anti)deuterons, denoted as d^\pm . The distributions are significantly different from the π^\pm case. According to the simulation, the 1 GeV (anti)deuterons should be measured on average with the time delay of 0.7 – 1.4 ns between the last and first layers. The value of 0.7 ns was estimated from the mean position of the Landau distribution used to fit the d^\pm curve presented in Figure 2(a), while 1.4 ns was obtained from the mean of this distribution. Even for the most conservative 0.7 ns value, there is an indication that 1 GeV deuterons can be separated from pions that have 0.5 ns time difference. Such a separation can be observed when using a tens-of-picosecond detector. For the 10 GeV particles presented in Figure 2(b), no separation between d^\pm and π^\pm can be observed.

In summary, we have illustrated that a typical difference between TL2 and TL1 (which is approximated by the difference between the last and first ECAL layer) is

¹The Monte Carlo studies used in this paper does not include simulations of calorimeter electronics.

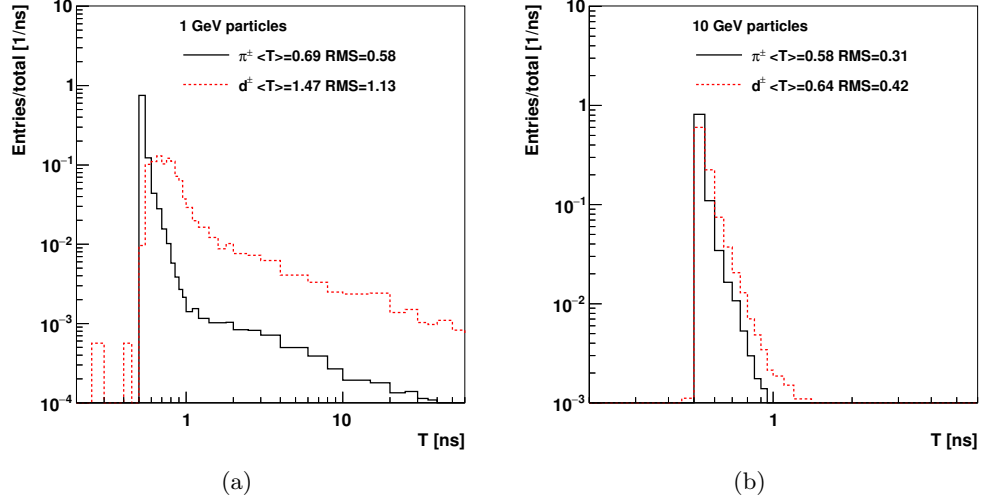


Figure 2: The difference between time of hits between the last and first layer of ECAL for single pions and deuterons with a transverse momentum of (a) 1 GeV and (b) 10 GeV. Only first (fastest) hits were considered to calculate the difference in TOF.

138 sufficient for particle identification using the TOF. As an example, a d^\pm can be identified
 139 and separated from pions for the momentum less than 1 GeV. This means that particles
 140 heavier than deuterons should be identified for a momentum larger than 1 GeV. In the
 141 following, we will abstract from the Geant4 simulations and calculate the kinematic
 142 regions where the identification of heavy stable particles using timing layers is possible.

3. Timing layers for single particles

Now let us discuss the kinematic regions for the TOF measurements in relation to either SM particles or BSM particles. Instead of the full Geant4 simulations, we will use a semi-analytic approach.

For an estimation of the separation power between different mass hypotheses, we will calculate the mass and momentum for which one can achieve a separation significance higher than 3σ (or $p\text{-val} < 0.03$). If there are two particles with a mass m and a reference (fixed) mass m_F , the 3σ separation can be achieved for this condition [10]:

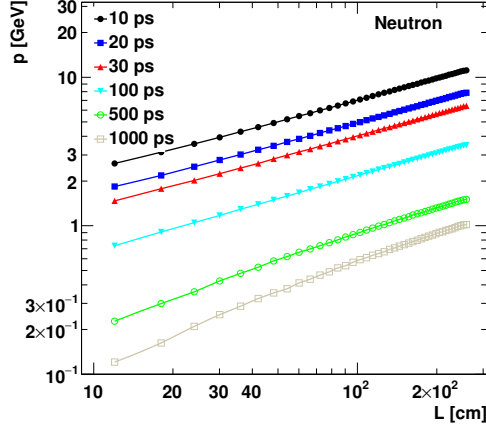
$$\frac{L}{c\sigma_{\text{TOF}}} \left| \sqrt{1 + \frac{m^2}{p^2}} - \sqrt{1 + \frac{m_F^2}{p^2}} \right| > 3 \quad (1)$$

where p is the momentum of a particle with a mass m , L is the length of the particle's trajectory, and σ_{TOF} is the resolution of the timing layer that measures the TOF.

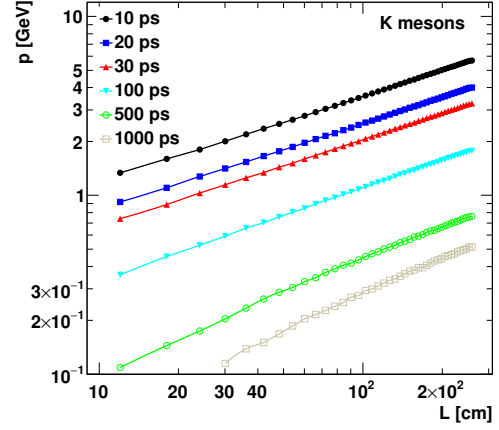
Figure 3 shows the 3σ separation from the pion mass hypothesis ($m_F = m_\pi$) using the same procedure as discussed in [10]. The calculations are performed for several options for the resolution of the timing layer, from 10 ps to 1 ns, as a function of the travel length L and the momenta. For a 20-ps detector and for a typical travel distance of $L \sim 1.5 - 2$ m from the interaction point to the electromagnetic calorimeter, neutrons (and protons) can be separated from the pion hypothesis up to 7 GeV. The separation of K -mesons can be performed up to 3 GeV. This momentum range should be sufficient for a reliable particle identification in a wide momentum range for physics studies focused on single-particle reconstruction. This can also be used for jets that are dominated by this momentum range of separate particles. For a detector with a 1 ns, the separation can only be possible up to 300 – 500 MeV. This is smaller than a typical minimum momentum of 0.5 GeV for particles considered for high-energy proton colliders. Therefore, a timing layer with 1-ns resolution cannot effectively be used for particle identification in such experiments.

Having discussed a rather classical case of identification of neutrons (or protons) and the K -mesons from the pion hypothesis, let us turn to the BSM searches for heavy particles. The most abundant SM background for light BSM particles from primary interactions are protons and neutrons. Other stable particles, that can be produced mainly in detector material (or in the interactions in the beam pipe) and detected by calorimeter are deuterons and α particles (composed of two protons and two neutrons). Although the rate of the α particles is low since they can easily be stopped by detector material, it is not impossible that the residual rate of such particle may still represent background for BSM searches that have a small production rate. Therefore, we will choose $m_F = m_\alpha \simeq 3.73$ GeV as a reference² in Eq. 1, and evaluate the 3σ separation for a wide range of masses and momentum starting from 4 GeV. For many planned experiments the distance between the interaction point and the first layer of the electromagnetic calorimeter is 1.5 – 2.5 m. Therefore, for a representative purpose, we will use $L = 2$ m and consider 0.2 m for the separation distance between the TL2 and TL1 timing layers.

²We should emphasize that this choice of α particles for the reference mass scale is arbitrary and is only motivated by our attempt to check the 3σ separation in the momentum region < 10 GeV.

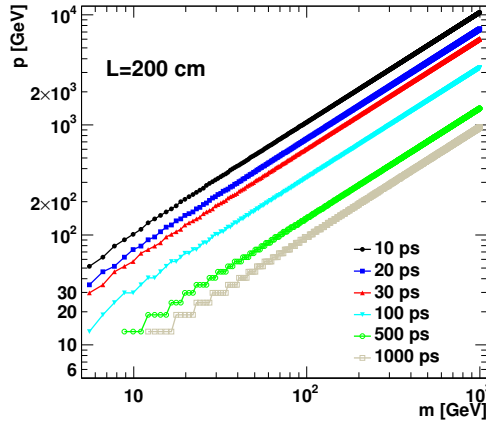


(a) Neutrons

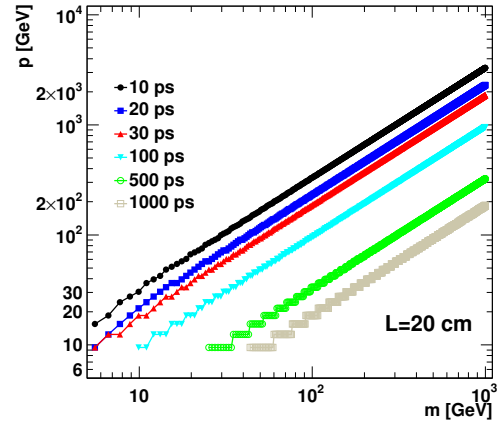


(b) K -mesons

Figure 3: The 3σ separation from the pion mass hypothesis for neutrons and K -mesons as a function of the length of the particle's trajectory L and the momentum p . For neutral particles the value of L approximately corresponds the distance between the interaction point and the surface of the ECAL for $\eta = 0$.



(a) for $L = 2$ m



(b) for $L = 0.2$ m

Figure 4: The 3σ separation from α particles for heavy particles assuming timing layers with different resolutions for TOF, and using (a) $L = 2$ m and (b) $L = 0.2$ m. The first value of L approximately equals to a typical distance from the interaction vertex to the first layer TL1, while the second value is the typical distance between two timing layers enclosing an electromagnetic calorimeter, assuming a typical calorimeter based on the silicon technology.

Figure 4 shows the particle identification power for different choices of the timing layer resolution and the travel distance L (see Fig. 1). For $L = 2$ m, which approximately corresponds to the distance from the interaction point and the TL1 when a particle travels at $\eta = 0$, one can see that a stable heavy particle with a mass of 100 GeV can be reconstructed up to 400 GeV assuming a 20-ps timing layer, but only up to 50 GeV using the standard 1-ns readout for time measurement.

In the case when TOF is measured between the two layers, TL1 and TL2, assuming a successful spacial match of the hits, the knowledge of the interaction vertex is not required. This type of measurements can be beneficial for neutral particles in collisions with large pile-up (multiple number of vertexes). The identification power in the case when the travel distance $L = 0.2$ m, i.e. when it is close to the distance between TL2 and TL1, is shown in Figure 4(b). For a stable particle with a mass of 100 GeV, the identification is possible up to 100 GeV in momentum. The standard calorimeter with 1 ns resolution can only perform the identification up to 20 GeV.

4. Showcase for the Dark QCD model

The arguments discussed before can be illustrated using a concrete physics scenario for BSM models. In particular, we will consider the dark QCD model [11, 12] which predicts “emerging” jets that are created in the decays of new long-lived neutral particles (dark hadrons), produced in a parton-shower process by dark QCD. The process includes two mediators with masses Mx , each of which decays to a Standard Model quark and a dark quark. The final-state signature consists of four high transverse momentum jets, two of which are from two from dark quarks. These two “emerging” jets contain many displaced vertices arising from the decays of the dark pions produced in the dark parton shower.

Recently searches for such emerging jets have been performed [13] by the CMS Collaboration. The emerging jet contains multiple displaced vertices and multiple tracks with large impact parameters. Assuming that the mass of the dark pion is 5 GeV, the signal acceptance using this approach does not exceed 40% at large masses of the mediators (see Figure 4 of [13]). Dark pion decay length defines the distance from the interaction point where a jet emerges. The emerging jet contains multiple displaced vertices, which are reconstructed using a tracker [13].

Alternatively, emerging jets can be reconstructed using calorimeters with high-resolution time measurements. This method is expected to have advantage for dark pions with a large decay length, i.e. in the situation when the tracker cannot be efficient in reconstructing tracks. It was also pointed out [12] that the emerging jets may have significant fraction of neutral particles and the reconstruction using charged tracks can have a low acceptance.

To estimate the performance of the timing layers in reconstructing emerging jets, we will use the same Monte Carlo settings as for Ref. [13]: The pp collision event samples are generated with the “hidden valley” model framework in PYTHIA 8.2 assuming the centre-of-mass energy of 13 TeV, a fixed mass of 5 GeV for the dark pions. The samples were created after changing the decay distance $c\tau$ of the dark pions. The mass Mx of the mediator was also varied.

225 To calculate the acceptance, will use the formalism based on Eq. 1, where $L = c\tau$,
 226 and m is the mass of the dark pion, i.e. L can be considered as a travel distance.
 227 After the dark pion creates a SM jet, we assume that such jets travel to the surface
 228 of the timing layer with the same speed for all values of m . For the timing layers,
 229 the signature of emerging jets is time delays compared to the other SM jets. The
 230 production vertex cannot be observed by the timing layers if such jets emerges before
 231 TL1³. After events being generated, the weighted average of the decay distances of
 232 all particles that originate from the dark pions, using the particle momentum as the
 233 weight, were calculated. This decay distance is used to approximate the decay length,
 234 without using a jet reconstruction. The calculation for the 3σ separation assumed
 235 $m_F = m_\alpha \simeq 3.73$ GeV although such a choice can be rather arbitrary. This value of
 236 m_F is used to give a conservative estimate of the arrival time of the SM jets. (One can
 237 argue that the SM jets mainly consist of light-flavour hadrons and photons, therefore,
 238 m_F is significantly lower).

239 The acceptance of reconstruction of the emerging jets events was calculated by
 240 counting the number of events that pass the Eq. 1 condition with the parameters as
 241 discussed before, divided by the total number of entries without this requirement. Fig-
 242 ure 5 shows the acceptance as a function of the mediator mass Mx and the decay
 243 distance of the dark pions. This figure can directly be compared to the similar accep-
 244 tance figure for the method based on tracks [13]. The acceptance based on the TOF
 245 is significantly larger for low Mx and large $c\tau$ of the pions, compared to a similar ac-
 246 ceptance distribution based on tracking information. The acceptance is larger for the
 247 timing layers smaller than 100 ns, than for the standard 1 ns calorimeter resolution.

248 Now we will be interested in the acceptance of the reconstruction of dark pions
 249 as a function of their mass and their lifetime, but assuming a fixed mass Mx for the
 250 mediator. This time we will consider the HE-LHC environment with pp collisions at
 251 the centre-of-mass energy of 27 TeV. The Monte Carlo settings for the signal model
 252 were similar to those discussed in [13], but then were further tuned [14] to obtain
 253 samples which were most suitable for the detector performance studies. The mass of
 254 the mediator was set to 10 TeV, while the mass of the dark pion was varied in the
 255 range between 5 and 1000 GeV. The dark pion proper decay length, $c\tau$, was varied
 256 between 1 mm and 1000 mm (independent of its mass). Other parameters were also
 257 appropriately modified to allow a sufficient phase space for the dark meson production.
 258 The mass of the dark pion is assumed to be one half the mass of the dark quark. The
 259 mass of the dark ρ is four times of the dark pion mass. The width of the mediator
 260 particle is assumed to be small as compared to the detector mass resolution.

261 As before, the acceptance of reconstruction of the emerging jets by measuring the
 262 timing information was calculated by counting the number of events that pass the
 263 Eq. 1 condition with the parameters as discussed before, divided by the total number
 264 of entries without this requirement. Figure 6 shows the efficiency as a function of $c\tau$
 265 and the mass of the dark pion. It can be seen that a detector with the standard 1 ns
 266 resolution does not have acceptance for the dark meson measurements. The acceptance
 267 is significantly larger for the timing layers that have a resolution smaller than 100 ns.

³It is possible that if such jets are created in the area between TL1 and TL2, such signatures can also be detected, but we will not consider this case.

268 The acceptance is small for low $c\tau$ or small masses, which is the expected feature of
269 the timing measurement. The timing layers with 20 ps have have 100% acceptance for
270 large values of $c\tau$ and dark-meson masses. The efficiency as a function of the particle
271 velocity for 20 ps and 1 ns timing layer resolutions is shown in the Appendix [Appendix](#)
272 [A](#).

273 Note that these results are relatively general since they are independent of the posi-
274 tion of the timing layers, and other details relevant to the geometry of the calorimeter.

275 5. Summary

276 This paper discusses the benefits of the timing layers positioned in front of the
277 hadronic calorimeters. Using the full Geant4 simulations and a semi-analytic approach,
278 the figures of merits for identification of single particles using timing layers with res-
279 olutions of 10 ps – 1 ns were calculated. It was illustrated how such layers can be
280 used for single particle identification and identification of heavy long-lived particles in
281 the context of the dark QCD model. It was shown that the timing layers lead to a
282 significant benefit for reconstruction of heavy long-lived particles in the region of $c\tau$
283 and momentum where track measurements have low reconstruction acceptance.

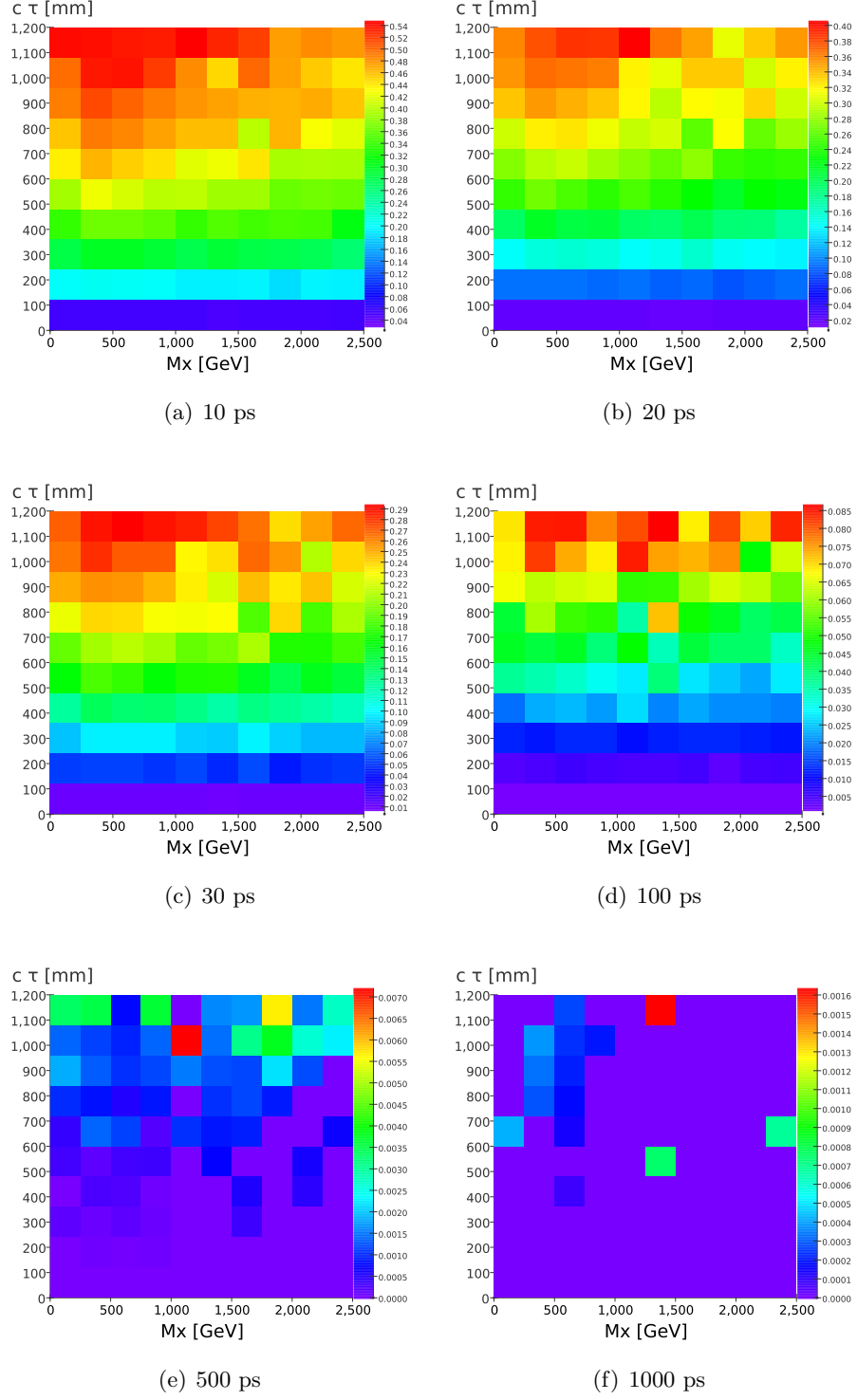


Figure 5: The acceptance for the reconstruction of emerging jets using the timing layers with different timing resolutions as a function of the mediator mass Mx and the $c\tau$ of the dark pions with the mass 5 GeV. The Pythia8 simulations are performed for the pp collisions at $\sqrt{s} = 13$ TeV.

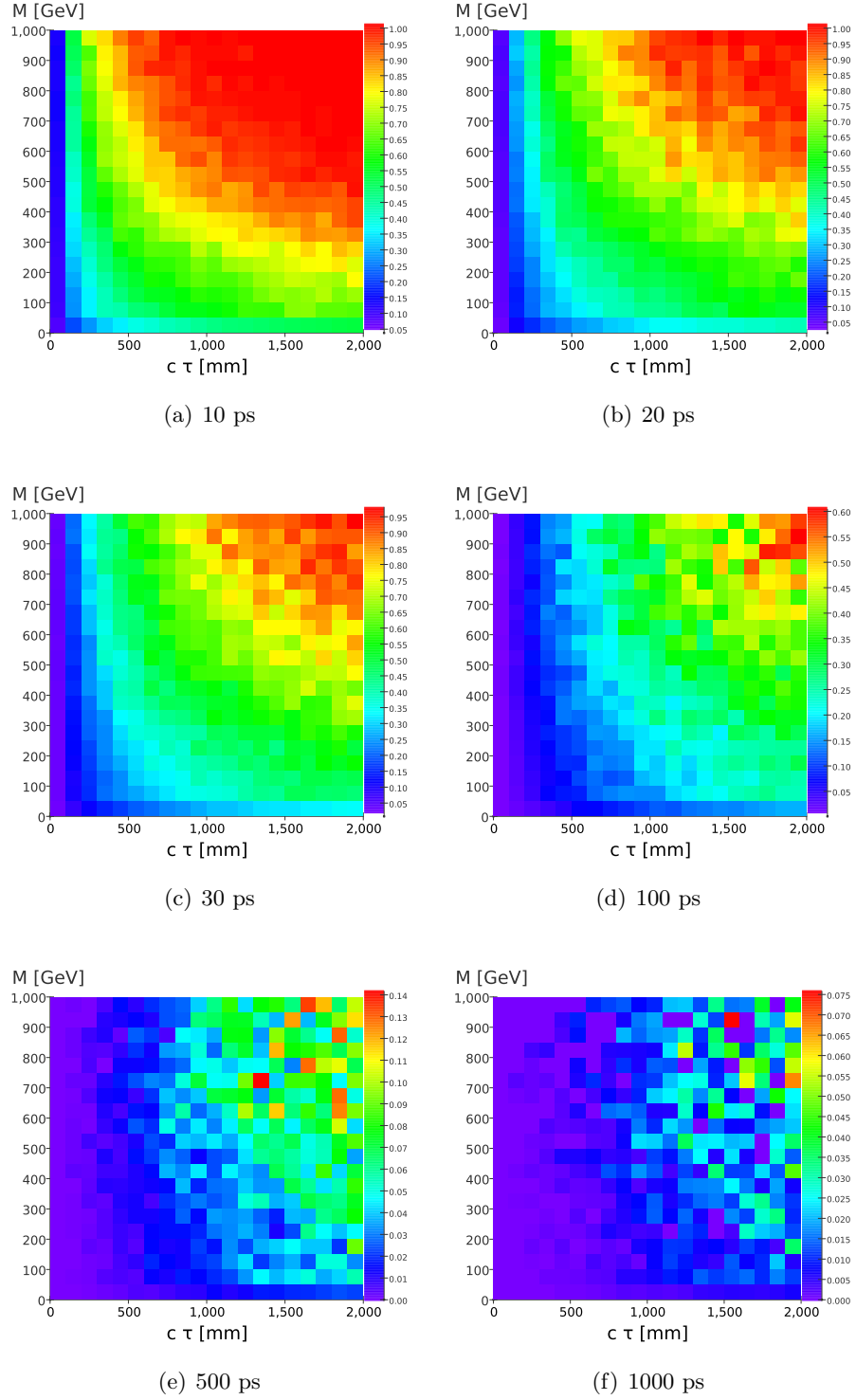


Figure 6: The acceptance for the reconstruction of emerging jets using the timing layers with different timing resolutions as a function of the mass of the dark pions and their $c\tau$. The mediator mass was fixed to 10 TeV. The Pythia8 simulations are performed for the pp collisions at $\sqrt{s} = 27$ TeV.

- [1] L. Linssen, A. Miyamoto, M. Stanitzki, H. Weerts, [Physics and Detectors at CLIC: CLIC Conceptual Design Report](#), CERN Yellow Reports: Monographs, CERN, Geneva, 2012, comments: 257 p, published as CERN Yellow Report CERN-2012-003. [doi:10.5170/CERN-2012-003](#). URL <http://cds.cern.ch/record/1425915>
- [2] T. Behnke, J. E. Brau, B. Foster, J. Fuster, M. Harrison, J. M. Paterson, M. Peskin, M. Stanitzki, N. Walker, H. Yamamoto, The International Linear Collider Technical Design Report - Volume 1: Executive Summary [arXiv:1306.6327](#).
- [3] M. Benedikt, [The Global Future Circular Colliders Effort](#) CERN-ACC-SLIDES-2016-0016. Presented at P5 Workshop on the Future of High Energy Physics, BNL, USA, Dec. 15-18, 2013. URL <http://cds.cern.ch/record/2206376>
- [4] J. Tang, et al., Concept for a Future Super Proton-Proton Collider (2015). [arXiv:1507.03224](#).
- [5] Z. Ahmed, et al., [New Technologies for Discovery](#), in: CPAD Instrumentation Frontier Workshop 2018: New Technologies for Discovery IV (CPAD 2018) Providence, RI, United States, December 9-11, 2018, 2019. [arXiv:1908.00194](#). URL <https://lss.fnal.gov/archive/2019/conf/fermilab-conf-19-487-di-nd-ppd-scd.pdf>
- [6] ATLAS Collaboration, [Technical Proposal: A High-Granularity Timing Detector for the ATLAS Phase-II Upgrade](#), Tech. Rep. CERN-LHCC-2018-023. LHCC-P-012, CERN, Geneva (Jun 2018). URL <http://cds.cern.ch/record/2623663>
- [7] F. Ferri, [The cms ecal phase-2 upgrade for high precision energy and timing measurements](#), Nuclear Instruments and Methods in Physics Research Section A: Accelerators, Spectrometers, Detectors and Associated Equipment 958 (2020) 162159, proceedings of the Vienna Conference on Instrumentation 2019. [doi:https://doi.org/10.1016/j.nima.2019.04.113](#). URL <http://www.sciencedirect.com/science/article/pii/S0168900219306102>
- [8] J. Allison, et al., Recent developments in Geant4, Nuclear Instruments and Methods in Physics Research A 835 (2016) 186.
- [9] S. V. Chekanov, M. Beydler, A. V. Kotwal, L. Gray, S. Sen, N. V. Tran, S. S. Yu, J. Zuzelski, Initial performance studies of a general-purpose detector for multi-TeV physics at a 100 TeV pp collider, JINST 12 (06) (2017) P06009. [arXiv:1612.07291](#), [doi:10.1088/1748-0221/12/06/P06009](#).
- [10] O. Cerri, S. Xie, C. Pena, M. Spiropulu, Identification of Long-lived Charged Particles using Time-Of-Flight Systems at the Upgraded LHC detectors, JHEP 04 (2019) 037. [arXiv:1807.05453](#), [doi:10.1007/JHEP04\(2019\)037](#).
- [11] Y. Bai, P. Schwaller, Scale of dark QCD, Phys. Rev. D89 (6) (2014) 063522. [arXiv:1306.4676](#), [doi:10.1103/PhysRevD.89.063522](#).
- [12] P. Schwaller, D. Stolarski, A. Weiler, Emerging Jets, JHEP 05 (2015) 059. [arXiv:1502.05409](#), [doi:10.1007/JHEP05\(2015\)059](#).
- [13] CMS Collaboration, A. M. Sirunyan, et al., Search for new particles decaying to a jet and an emerging jet, JHEP 02 (2019) 179. [arXiv:1810.10069](#), [doi:10.1007/JHEP02\(2019\)179](#).
- [14] K. Pedro, P. Schwaller, Private communication. We thank Dr. P. Kevin and P. Schwaller for help with the setup of Monte Carlo generation parameters.

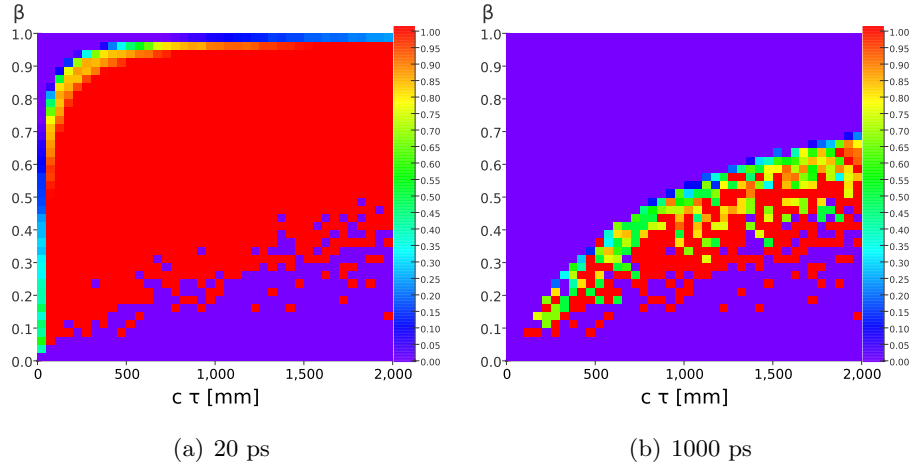


Figure A.7: The efficiency for the reconstruction of emerging jets using the timing layers with different timing resolutions. The plot shows the efficiency as a function of $c\tau$ and the particle velocity β

323 Appendices

324 Appendix A. Appendix

325 Figure A.7 shows the reconstruction efficiency as a function of $c\tau$ and the particle
 326 velocity $\beta = |p|/E$, for the two extreme cases of the timing layers.